Geophysical Journal International

Geophys. J. Int. (2011) **186,** 1315–1330 doi: 10.1111/j.1365-246X.2011.05110.x

Seismic response of a single and a set of filled joints of viscoelastic deformational behaviour

J. B. Zhu,[1] A. Perino,[2] G. F. Zhao,[3] G. Barla,[2] J. C. Li,[4] G. W. Ma[5] and J. Zhao[1]

[1] *Ecole Polytechnique Fédérale de Lausanne (EPFL), School of Architecture, Civil and Environmental Engineering (ENAC), Laboratory for Rock Mechanics (LMR), EPFL-ENAC-LMR, Station 18,* CH-1015 *Lausanne, Switzerland. E-mail: jian.zhao@epfl.ch*

[2] *Department of Structural and Geotechnical Engineering, Politecnico di Torino, Corso Duca degli Abruzzi 24,* 10129*, Torino, Italy*

[3] *School of Civil and Environmental Engineering, University of New South Wales, Sydney, NSW* 2052*, Australia*

[4] *State Key Laboratory of Geomechanics and Geotechnical Engineering, Institute of Rock and Soil Mechanics, Chinese Academy of Sciences, Wuhan,* 430071*, China*

[5] *School of Civil and Resource Engineering, University of Western Australia, 35 Stirling Highway, Crawley* WA6009*, Australia*

Accepted 2011 June 9. Received 2011 May 12; in original form 2011 February 21

SUMMARY

Rock joints are often filled with weak medium, for example, saturated clay or sand, of viscoelastic nature. Their effects on wave propagation can be modelled as displacement and stress discontinuity conditions. The viscoelastic behaviour of the filled joint can be described by either the Kelvin or the Maxwell models. The analytical solutions for wave propagation across a single joint are derived in this paper by accounting for the incident angle, the non-dimensional joint stiffness, the non-dimensional joint viscosity and the acoustic impedance ratio of the filled joint. It is shown that the viscoelastic behaviour results in dissipation of wave energy and frequency dependence of the reflection and transmission coefficients. Based on curve fitting of the experimental data of *P*-wave propagation across a single joint filled with saturated sand, both the Kelvin and Maxwell models are found to reproduce the behaviour of the filled joint, in terms of the amplitude and frequency contents. Then, wave transmission across a filled joint set is studied with the virtual wave source method and the scattering matrix method, where multiple wave reflections among joints are taken into account. It is shown that the non-dimensional joint spacing and the number of joints have significant effects on the transmission coefficients.

Key words: Body waves; Seismic anisotropy; Seismic attenuation; Wave propagation; Rheology and friction of fault zones.

1 INTRODUCTION

Joints, which are parallel fractures, are important mechanical features of rock masses. When a wave propagates through a rock mass, the wave attenuation is mainly due to the presence of joints (King *et al.* 1986). Many studies have been performed on wave propagation across non-filled joints (Schoenberg 1980; Cai & Zhao 2000). Natural joints, however, are often filled with saturated sand, clay, soil or weathered rock of viscoelastic deformational behaviour, and hence, wave propagation across them needs to be studied. This is of great importance in geophysics, earthquake engineering, non-destructive evaluation and rock mechanics.

With the layered medium model, a filled joint is treated as a perfectly bonded thin layer sandwiched between two background half-spaces. The sandwiched thin layer can be elastic (Brekhovskikh 1980) or viscoelastic (Fehler 1982). Across the two interfaces between the filled thin layer and the background half-spaces, both the displacements and stresses are continuous. However, the reflection and transmission coefficients across a filled joint are very complicated, especially when multiple wave reflections between the two interfaces are taken into account.

The wave scattering theory treats the filled joint as a plane boundary with a distribution of small cracks and voids (Hudson *et al.* 1996). Wave propagation across the filled joint is determined by crack geometry, crack distribution, crack density, saturation and other parameters. The fact that detailed crack distribution, geometry and density are difficult to derive limits the application of the wave scattering theory to the seismic response of filled joints.

The displacement discontinuity model (Schoenberg 1980; Pyrak-Nolte *et al.* 1990) and the displacement and velocity discontinuity model (Pyrak-Nolte *et al*. 1990; Suárez-Rivera 1992) treat the joint as a non-welded interface across which stresses are continuous, but displacements are discontinuous. However, given that the density of the filled medium is not negligible compared with the density of the

half-spaces, the initial mass of the filled joint should be taken into account, and the stresses across it considered to be discontinuous (Rokhlin & Wang 1991).

Wave propagation across a single joint has been extensively studied (Schoenberg 1980; Pyrak-Nolte *et al*. 1990; Gu *et al.* 1996a). However, when multiple parallel joints are present, wave propagation will be more complicated due to multiple wave reflections among joints (Schoenberger & Levin 1974; Cai & Zhao 2000; Zhao *et al*. 2006a,b,c).

In this paper, combined with the displacement and stress discontinuity model, the complete analytical solutions for wave propagation across a single filled joint of viscoelastic behaviour are first derived, where the joint is described by the Kelvin and the Maxwell models. Then, parametric studies on the magnitude of reflection and transmission coefficients and energy loss across a single filled joint are performed. Subsequently, with reference to modified split Hopkins pressure bar experimental data on *P*-wave propagation across a joint filled with saturated sand, curve fitting between the measured spectral amplitudes and predicted spectral amplitudes is performed. Finally, wave propagation across a filled joint set of viscoelastic behaviour is studied with the virtual wave source method (VWSM) and the scattering matrix method (SMM), where multiple wave reflections among joints are considered.

2 ANALYTICAL SOLUTIONS FOR WAVE PROPAGATION ACROSS A SINGLE FILLED JOINT OF VISCOELASTIC BEHAVIOUR

The incident as well as the reflected and transmitted harmonic waves are represented, in vector form, by

$$\mathbf{u}_n = A_n \mathbf{b}_n \exp[(\mathrm{i}\omega/C_n)\mathbf{p}_n \cdot \mathbf{X} - \mathrm{i}\omega t], \tag{1}$$

where $\mathbf{u}_n$ is the particle displacement vector, A_n is the wave amplitude, $\mathbf{b}_n$ is the wave motion unit vector, C_n is the wave velocity, $\mathbf{p}_n$ is the wave number unit vector, $\mathbf{X}$ is the position vector, the subscript n denotes different waves including incident *P*-wave (*IP*), incident *SV*-wave (*ISV*), incident *SH*-wave (*ISH*), reflected *P*-wave (*RP*), reflected *SV*-wave (*RSV*), reflected *SH*-wave (*RSH*), transmitted *P*-wave (*TP*), transmitted *SV*-wave (*TSV*) and transmitted *S*-wave (*TSH*). Fig. 1 shows the incident, reflected and transmitted waves upon one joint, where the media of opposite sides of the joint are assumed to be identical.

Thus, for incident *P*-wave : $\mathbf{p}_{IP} = \sin\theta\mathbf{i} - \cos\theta\mathbf{k},\ \mathbf{b}_{IP} = \mathbf{p}_{IP}.$ (2)

For incident *SV*-wave : $\mathbf{p}_{ISV} = \sin\phi\mathbf{i} - \cos\phi\mathbf{k},\ \mathbf{b}_{ISV} = \mathbf{j} \times \mathbf{p}_{ISV}.$ (3)

For incident *SH*-wave : $\mathbf{p}_{ISH} = \sin\phi\mathbf{i} - \cos\phi\mathbf{k},\ \mathbf{b}_{ISH} = \mathbf{j}.$ (4)

For reflected *P*-wave : $\mathbf{p}_{RP} = \sin\theta\mathbf{i} + \cos\theta\mathbf{k},\ \mathbf{b}_{IP} = \mathbf{p}_{IP}.$ (5)

For reflected *SV*-wave : $\mathbf{p}_{RSV} = \sin\phi\mathbf{i} + \cos\phi\mathbf{k},\ \mathbf{b}_{RSV} = \mathbf{j} \times \mathbf{p}_{RSV}.$ (6)

For reflected *SH*-wave : $\mathbf{p}_{RSH} = \sin\phi\mathbf{i} + \cos\phi\mathbf{k},\ \mathbf{b}_{RSH} = \mathbf{j}.$ (7)

For transmitted *P*-wave : $\mathbf{p}_{TP} = \sin\theta\mathbf{i} - \cos\theta\mathbf{k},\ \mathbf{b}_{TP} = \mathbf{p}_{TP}.$ (8)

For transmitted *SV*-wave : $\mathbf{p}_{TSV} = \sin\phi\mathbf{i} - \cos\phi\mathbf{k},\ \mathbf{b}_{TSV} = \mathbf{j} \times \mathbf{p}_{TSV}.$ (9)

For transmitted *SH*-wave : $\mathbf{p}_{TSH} = \sin\phi\mathbf{i} - \cos\phi\mathbf{k},\ \mathbf{b}_{TSH} = \mathbf{j}.$ (10)

where $\mathbf{i}$, $\mathbf{k}$ and $\mathbf{j}$ is the unit vector in the x, z and y direction.

When the density of the filled material is not negligible compared with the rock density, the initial mass of the filled joint can affect wave propagation (Rokhlin & Wang 1991). With the consideration of the initial mass terms of the filled joint, besides the displacements, the stresses across the filled joint are also discontinuous. In fact, the density of the filled material, which is usually saturated sand or clay, is comparable with the rock density. Therefore, the displacement discontinuity model (Schoenberg 1980; Pyrak-Notle *et al.* 1990) is not appropriate to study wave propagation across filled joints. The boundary conditions to represent the filled joint used in this study are termed as the displacement and stress discontinuity model. It should be pointed out that the displacement discontinuity is the generalized form of velocity discontinuity.

The Kelvin model (one spring and one dashpot in parallel) is usually adopted to describe the dynamic and seismic response of saturated soil (Verruijt 2010; Das & Ramana 2011). However, Suárez-Rivera (1992) found that the Maxwell model (one spring and one dashpot in series) is better for studying shear wave propagation across a thin clay layer. In this study, both joints of the Kelvin and the Maxwell viscoelastic deformational behaviours are studied. To be convenient, we will term the joint of the Kelvin and the Maxwell viscoelastic deformational behaviour as the Kelvin joint and the Maxwell joint, respectively.

With the displacement and stress discontinuity model, the boundary conditions (see Fig. 1) are

$$\tau_{zz}^a - \tau_{zz}^b = -\omega^2 m_n u_z^b, \tag{11}$$

$$\tau_{zx}^a - \tau_{zx}^b = -\omega^2 m_t u_x^b, \tag{12}$$

$$u_z^a - u_z^b = \left(\frac{1}{\kappa_n - \mathrm{i}\omega\eta_n}\right)\tau_{zz}^b, \tag{13}$$

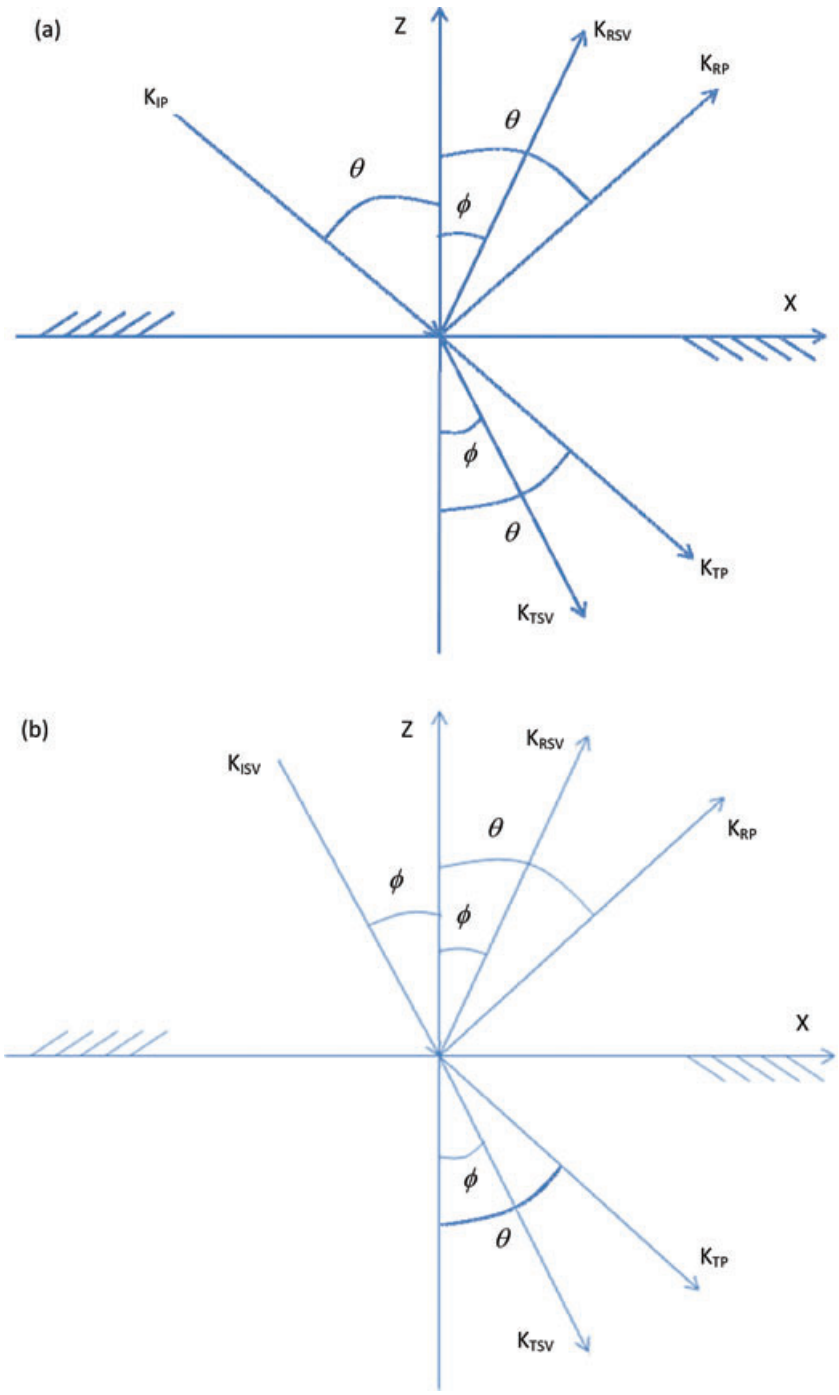

Figure 1. Incident, reflected and transmitted waves upon a joint for (a) *P*-wave incidence; (b) *SV*-wave incidence and (c) *SH*-wave incidence.

$$u_x^a - u_x^b = \left(\frac{1}{\kappa_t - \mathrm{i}\omega\eta_t}\right)\tau_{zx}^b, \tag{14}$$

for a Kelvin joint, and

$$\tau_{zz}^a - \tau_{zz}^b = -\omega^2 m_n u_z^b, \tag{15}$$

$$\tau_{zx}^a - \tau_{zx}^b = -\omega^2 m_t u_x^b, \tag{16}$$

$$u_z^a - u_z^b = \left(\frac{1}{\kappa_n} - \frac{1}{\mathrm{i}\omega\eta_n}\right)\tau_{zz}^b, \tag{17}$$

$$u_x^a - u_x^b = \left(\frac{1}{\kappa_t} - \frac{1}{\mathrm{i}\omega\eta_t}\right)\tau_{zx}^b, \tag{18}$$

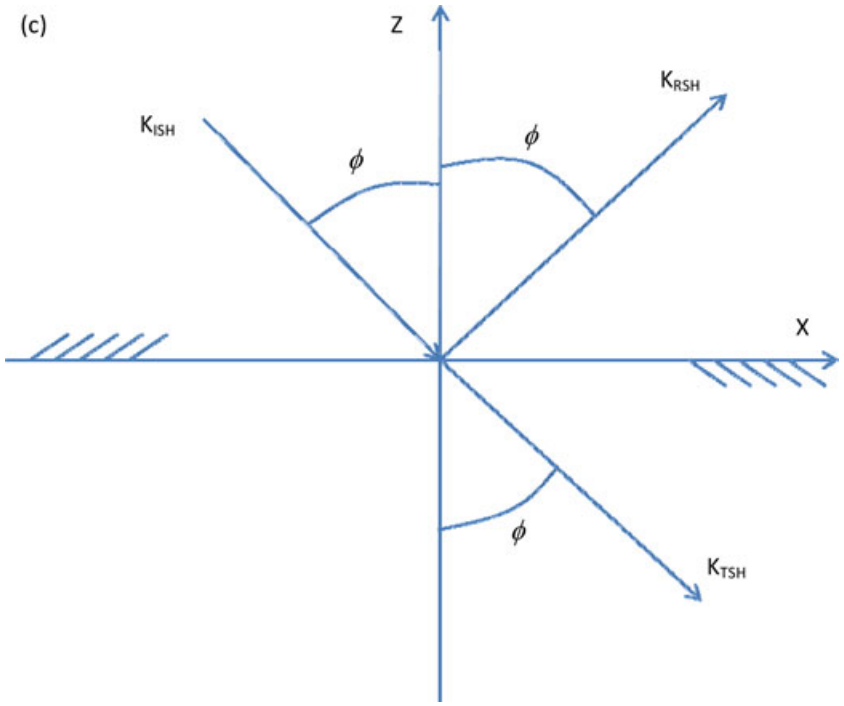

Figure 1. (*Continued*.)

for a Maxwell joint, where τ is the stress, the subscript *zz, zx, x* and *z* refer to the direction of stresses and displacements, the superscripts *a* and *b* refer to opposite sides of the joint, m_n is termed as the normal mass, m_t is termed as the tangential mass, κ_n and κ_t are the normal and shear joint specific stiffness, respectively, η_n and η_t are the normal and shear joint specific viscosity, respectively.

Here, $m_n = \rho_0 h$, which determines the stress difference in the normal direction, is the mass of the filled medium of a unit area of the joint plane and termed as the normal mass, where ρ_0 is the density of the filled medium, h is the joint thickness. $m_t = q m_n = [1 - (C_{\text{plate}}/C_i)^2 \sin^2 \chi_i] m_n$, which determines the stress difference in the tangential direction, is the effective mass in the tangential direction and named as the tangential mass. q is a parameter dependent on the plate velocity of the filled medium $C_{\text{plate}} = \sqrt{E_0/[\rho_0(1-\upsilon_0^2)]}$, where E_0 and υ_0 are Young's modulus and Poisson's ratio of the filled medium, respectively, the incident angle χ_i and the wave velocity of the rock corresponding to the type of the incident wave C_i ($C_i = C_P$, $\chi_i = \theta$ for *P*-wave incidence, or $C_i = C_S$, $\chi_i = \phi$ for *S*-wave incidence). When the wave is normally incident upon the joint, $q = 1$ and thus, $m_t = m_n$. The joint specific stiffness κ, which is defined as the ratio of stress to deformation with unit Pa m^{-1}, is different from the usually used joint stiffness defined as the ratio of force to deformation with unit N m^{-1}. The specific joint viscosity η, which is defined as the ratio of stress to flow velocity with unit Pa·s m^{-1}, is different from the usually used viscosity defined as the ratio of stress to flow velocity gradient with unit Pa·s.

With Hooke's law, the stresses can be obtained.

$$\tau_{zz} = \lambda \frac{\partial u_x}{\partial x} + (\lambda + 2\mu) \frac{\partial u_z}{\partial z}, \tag{19}$$

$$\tau_{zx} = \mu \left(\frac{\partial u_x}{\partial z} + \frac{\partial u_z}{\partial x} \right), \tag{20}$$

where λ and μ are Lamé's constants of the rock.

From eqs (1–20), the complete analytical solutions for the reflection and transmission coefficients across a single viscoelastic joint, in matrix form, are

$$A \begin{bmatrix} R_{P\to P} \\ R_{P\to SV} \\ T_{P\to P} \\ T_{P\to SV} \end{bmatrix} = B \tag{21}$$

for *P*-wave incidence,

$$A \begin{bmatrix} R_{SV\to P} \\ R_{SV\to SV} \\ T_{SV\to P} \\ T_{SV\to SV} \end{bmatrix} = C \tag{22}$$

for *SV*-wave incidence and

$$D\begin{bmatrix} R_{SH\to SH} \\ T_{SH\to SH} \end{bmatrix} = E \tag{23}$$

for *SH*-wave incidence, where *R* and *T* are reflection and transmission coefficients, respectively, the subscript means the type of incident wave (before the arrow) and the type of the reflected or transmitted waves across the joint (after the arrow), and

$$A = \begin{bmatrix} \cos 2\phi & -c\sin 2\phi & -\cos 2\phi + \mathrm{i}cd\cos\theta & -c\sin 2\phi + \mathrm{i}cd\sin\phi \\ c\sin 2\theta & \cos 2\phi & c\sin 2\theta - \mathrm{i}qd\sin\theta & -\cos 2\phi + \mathrm{i}qd\cos\phi \\ \cos\theta & -\sin\phi & \cos\theta - \dfrac{\mathrm{i}\cos 2\phi}{cK_n'} & \sin\phi - \dfrac{\mathrm{i}\sin 2\phi}{K_n'} \\ \sin\theta & \cos\phi & -\sin\theta + \dfrac{\mathrm{i}c\sin 2\theta}{K_t'} & \cos\phi - \dfrac{\mathrm{i}\cos 2\phi}{K_t'} \end{bmatrix}, \tag{24}$$

$$B = \begin{bmatrix} -\cos 2\phi \\ c\sin 2\theta \\ \cos\theta \\ -\sin\theta \end{bmatrix}, \tag{25}$$

$$C = \begin{bmatrix} -c\sin 2\phi \\ -\cos 2\phi \\ \sin\phi \\ \cos\phi \end{bmatrix}, \tag{26}$$

$$D = \begin{bmatrix} 1 & \dfrac{\mathrm{i}\cos\phi}{K_t'} - 1 \\ \mathrm{i}\cos\phi & \mathrm{i}\cos\phi + qd \end{bmatrix}, \tag{27}$$

$$E = \begin{bmatrix} -1 \\ \mathrm{i}\cos\phi \end{bmatrix}, \tag{28}$$

where $\frac{1}{K_n'} = \frac{1}{K_n - \mathrm{i}H_n}$ and $\frac{1}{K_t'} = \frac{1}{K_t - \mathrm{i}H_t}$ are effective joint stiffnesses for the Kelvin joint, $\frac{1}{K_n'} = \frac{1}{K_n} - \frac{1}{\mathrm{i}H_n}$ and $\frac{1}{K_t'} = \frac{1}{K_t} - \frac{1}{\mathrm{i}H_t}$ are effective joint stiffnesses for the Maxwell joint, $K_n = k_n/(\omega Z_S)$ and $K_t = k_t/(\omega Z_S)$ are the non-dimensional normal and tangential joint stiffness, respectively, $H_n = \eta_n/Z_S$ and $H_t = \eta_t/Z_S$ are the non-dimensional normal and tangential joint viscosity, respectively, Z_S is the rock impedance for *S*-wave, c is the ratio of the velocity of *S*-wave to that of *P*-wave and is determined by the Poisson ratio of the rock, $d = \frac{Z_e}{Z_S} = \frac{\omega m_n}{Z_s} = \frac{\omega\rho_0 h}{Z_s}$ is non-dimensional and termed as the impedance ratio of the filled joint, Z_e is the effective acoustic impedance of the filled medium, which can be regarded as the acoustic impedance of the filled medium when the wavelength is equal to $2\pi h$.

The solution for a purely elastic joint, corresponding to the case where the joint is non-filled and dry, or a purely viscous joint, corresponding to the case where there is one thin viscous liquid film in the joint and the joint plane is perfectly smooth, can be obtained from the solution for a Kelvin joint by setting the specific viscosity to zero or the specific stiffness to zero, respectively.

By setting the incident angles to be zero in eqs (21)–(28), the reflection and transmission coefficients for normally incident wave propagation across a single viscoelastic joint can be derived.

For normally incident *P* wave, the reflection and transmission coefficients across a single viscoelastic joint are

$$R_P = \frac{\mathrm{i}/K_{nP}' - \mathrm{i}d_P}{2 - \mathrm{i}d_P - \mathrm{i}/K_{nP}'}, \tag{29}$$

$$T_P = \frac{2}{2 - \mathrm{i}d_P - \mathrm{i}/K_{nP}'}, \tag{30}$$

where $d_P = \frac{Z_e}{Z_P} = \frac{\omega m_n}{Z_P} = \frac{\omega\rho_0 h}{Z_P}$, $\frac{1}{K_{nP}'} = \frac{1}{K_{nP} - \mathrm{i}H_{nP}}$ for the Kelvin joint, $\frac{1}{K_{nP}'} = \frac{1}{K_{nP}} - \frac{1}{\mathrm{i}H_{nP}}$ for the Maxwell joint, $K_{nP} = k_n/(\omega Z_P)$ is the non-dimensional normal joint stiffness for *P* wave, $H_{nP} = \eta_n/Z_P$ is the non-dimensional normal joint viscosity for *P* wave, Z_P is the rock impedance for *P* wave.

For normally incident *SV*-wave, the reflection and transmission coefficients across a single viscoelastic joint are

$$R_{SV} = \frac{\mathrm{i}/K_t' - \mathrm{i}d}{2 - \mathrm{i}d - \mathrm{i}/K_t'}, \tag{31}$$

$$T_{SV} = \frac{2}{2 - \mathrm{i}d - \mathrm{i}/K_t'}. \tag{32}$$

For normally incident *SH*-wave, the reflection and transmission coefficients are

$$R_{SH} = \frac{\mathrm{i}d - \mathrm{i}/K_t'}{2 - \mathrm{i}d - \mathrm{i}/K_t'}, \tag{33}$$

$$T_{SH} = \frac{2}{2 - \mathrm{i}d - \mathrm{i}/K_t'}. \tag{34}$$

Figs 2 and 3 show the magnitude of reflection and transmission coefficients across a Kelvin and a Maxwell joint, respectively, versus the incident angles for incident *P*, *SV* and *SH* waves. It is assumed that the *P*-wave velocity of the rock is 6131 m s^{-1}, the *S*-wave velocity of the rock is 3830 m s^{-1}, the plate velocity of the filled medium is 1000 m s^{-1}, all of which can be obtained when the Young's modulus and Poisson's ratio of the rock and the filled medium are known (Zhao 1996). Thus, $c = 0.6247$, the critical angle for *SV*-wave incidence is 38.66°, and q can be derived for the specific incident wave. Since interface waves will not be studied in detail, the *SV*-wave incident angle is confined to range from 0° to 38.66°. It is also assumed that $K_n = K_t = 1$, $H_n = H_t = 1$ and $d = 0.1$, which can correspond various combinations of rock material, rock joints, filled medium and incident waves.

As seen from Figs 2 and 3, for both the Kelvin and the Maxwell joints, when the incident angle of *P* wave and *SH* wave approaches 90°, $|R_{P\to P}|$ and $|R_{SH\to SH}|$ approach one, while the other reflection and transmission coefficients are vanishing. This indicates that all wave energy is reflected and conserved in the reflected wave with the same wave type as the incident wave when the wave incident direction is parallel to the joint plane. When the incident angle of *SV*-wave approaches the critical angle, except $|R_{SV\to SV}|$, the other reflection and transmission coefficients increase rapidly for both the Kelvin and the Maxwell joints. In fact, at the critical angle, a large-amplitude head wave is produced, and beyond the critical angle, inhomogeneous *P* interface wave is generated (Gu *et al.* 1996b).

Another interesting phenomenon is that $|R_{P\to P}|$, $|R_{SV\to SV}|$ and $|R_{SH\to SH}|$ approach zero for certain incident angles for both the Kelvin and the Maxwell joints. In fact, in some cases, $|R_{P\to P}|$, $|R_{SV\to SV}|$ and $|R_{SH\to SH}|$ can be exactly equal to zero for certain incident angles, which can be obtained by setting $|R_{P\to P}| = 0$, $|R_{SV\to SV}| = 0$ and $|R_{SH\to SH}| = 0$ in eqs (21)–(24). The general trend of reflection and transmission coefficients versus incident angles is similar for the Kelvin and the Maxwell joints, although the magnitudes can be quite different.

Besides the incident angle, the non-dimensional joint stiffness, the non-dimensional joint viscosity and the impedance ratio of the filled joint also affect the magnitude of reflection and transmission coefficients. Figs 4 and 5 show the magnitudes of reflection and transmission coefficients across a Kelvin joint and a Maxwell joint, respectively, as a function of K_{nP}, H_{nP} and d_P for normal *P*-wave incidence. The changing trend of the magnitudes of the reflection and transmission coefficients for normal *S*-wave incidence as a function of K_n, H_n and d is the same as that for normal *P*-wave incidence.

It is found that for both the Kelvin and the Maxwell joints, with increasing K_{nP} or H_{nP}, the magnitude of reflection coefficients is always non-increasing, while the magnitude of transmission coefficients is always non-decreasing except when H_{nP} is smaller than a value around one for the Kelvin joint.

The phenomenon that for the Kelvin joint, $|T_P|$ decreases with increasing H_{nP} when H_{nP} is smaller than certain value results from the wave dissipation due to the viscosity of the joint. As shown in Fig. 6(a), the wave energy loss is the largest when the value of H_{nP} is close to one. For the Kelvin joint, when either K_{nP} or H_{nP} approaches infinity, $|R_P|$ approaches zero, which indicates that all energy is transmitted and dissipated. For the Maxwell joint, when either K_{nP} or H_{nP} approach infinity, only the non-infinity H_{nP} or K_{nP} determine $|R_P|$ and $|T_P|$, and thus both $|R_P|$ and $|T_P|$ are approximately constant but non-zero.

From eqs (29) and (30), it can be found that for the Maxwell joint, $|R_P|$ approaches zero only when both K_{nP} and H_{nP} approach infinity. For both the Kelvin and the Maxwell joints, $|R_P|$ and $|T_P|$ change little with increasing d_P when d_P is small. While d_P is sufficiently large, $|T_P|$ approaches 1, while $|R_P|$ approaches zero. However, this phenomenon is only meaningful in mathematics. In nature, the value of d_P is usually small.

From eqs (29) and (30), it is found that $|R_P|^2 + |T_P|^2 < 1$, which is due to the energy dissipation from the viscosity and initial mass of the filled joint. Figs 6 and 7 show the energy loss ratio (e_{loss}), which is defined as the ratio of dissipated energy to the energy of the incident wave, across a Kelvin joint and a Maxwell joint, respectively, as a function of H_{nP} and d_P for normally incident *P* wave. The changing trend of e_{loss} for *S*-wave incidence is the same as that for *P*-wave incidence.

It is found that for both the Kelvin and the Maxwell joints, e_{loss} arrives at the maximum value when $\log_{10}(H_n^P)$ is close to zero. When H_n^P approaches zero, e_{loss} approaches zero for the Maxwell joint, but e_{loss} is non-zero for the Kelvin joint. It is because d_P does not result in any energy dissipation when H_{nP} approaches zero for the Maxwell joint, while d_P does for the Kelvin joint. When H_{nP} approaches infinity, e_{loss} approaches zero for the Kelvin joint, but e_{loss} is non-zero for the Maxwell joint. It is because d_P does not result in any energy dissipation when H_{nP} approaches infinity for the Kelvin joint, but d_P does for the Maxwell joint. For both the Kelvin and the Maxwell joints, with increasing d_P, e_{loss} first increases to the maximum value, then it decreases to zero. As mentioned before, it should be noted that the value of d_P is usually small in nature.

3 EXPERIMENTAL DATA AND CURVE FITTING

3.1 Experimental data

A modified split Hopkinson pressure bar (SHPB) test was performed to study wave propagation across a filled rock joint (Li & Ma 2009). As shown in Fig. 8, a sand layer was sandwiched between the incident and transmitted granite pressure bars. The two bars have 5 cm diameter

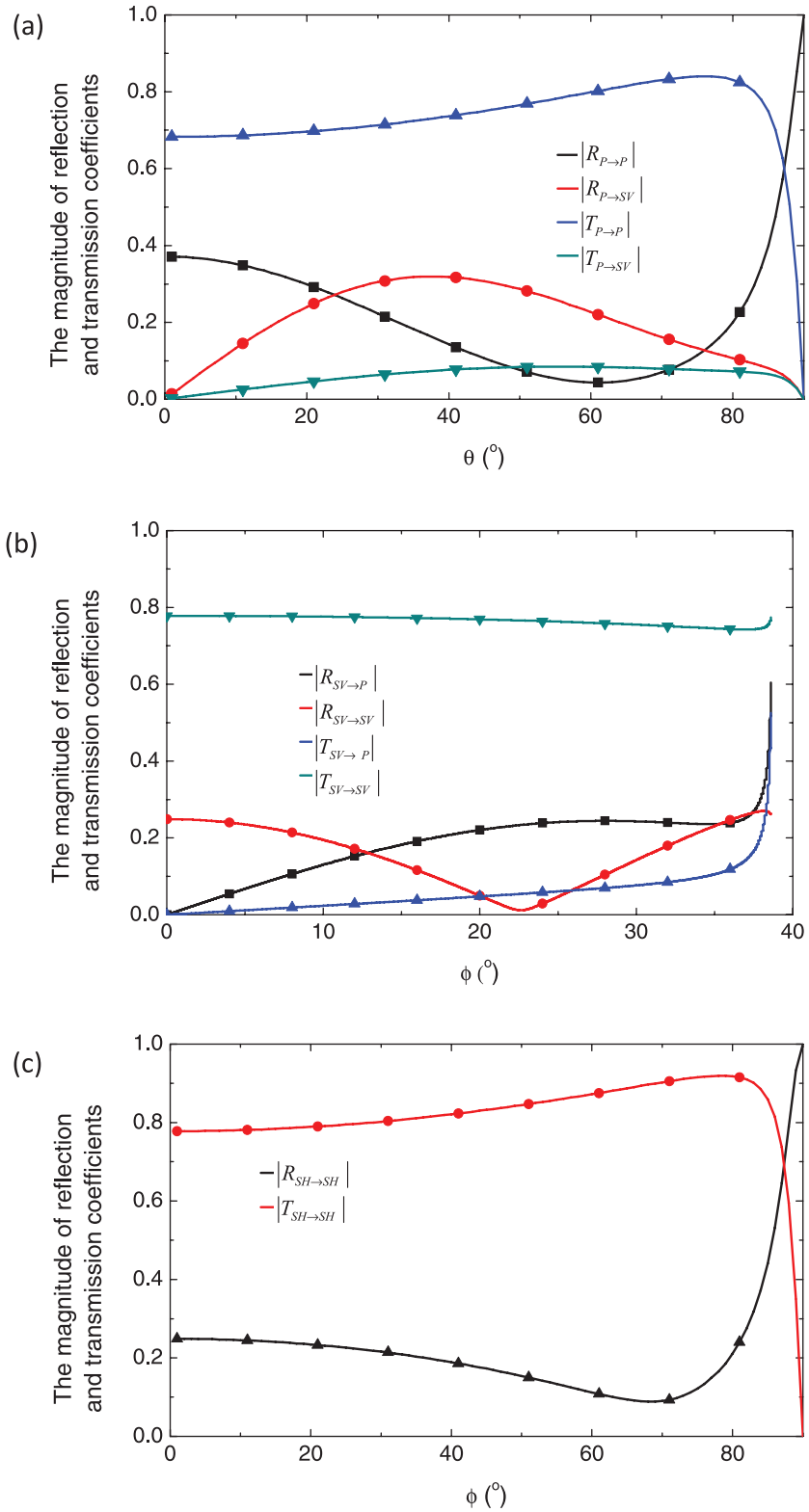

Figure 2. Reflection and transmission coefficients across a single Kelvin joint versus incident angles for (a) *P*-wave incidence; (b) *SV*-wave incidence and (c) *SH*-wave incidence.

and lengths 97 and 100.5 cm, respectively. A pendulum hammer is used to generate a *P*-wave pulse applied to the left boundary of the incident bar. The sand layer is contained in a plastic tube to prevent outflow of the sand. Four strain gauges are used to obtain the wave recordings. The density of the granite is 2650 kg m^{-3}, the *P*-wave velocity is 4758 m s^{-1}, the swing-angle of the hammer is 40°, the thickness of the filled joint is 3 mm, the water content and density of sand are 5 per cent and 1592.2 kg m^{-3}, respectively. With the measured wave recordings,

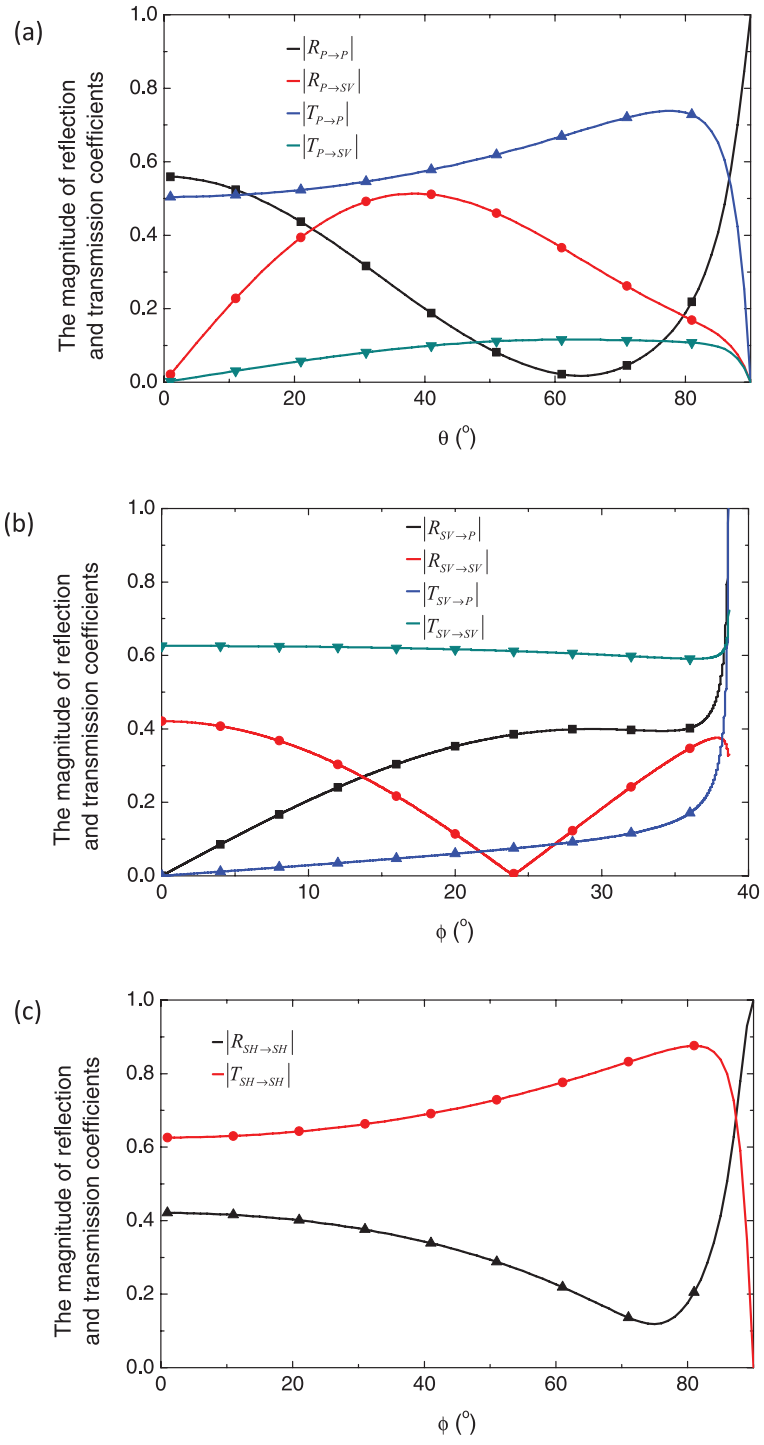

Figure 3. Reflection and transmission coefficients across a single Maxwell joint versus incident angles for (a) *P*-wave incidence; (b) *SV*-wave incidence and (c) *SH*-wave incidence.

incident, reflected and transmitted waves can be obtained after different waves are separated. Fig. 9 shows the incident and transmitted waves upon the filled joint.

3.2 Curve fitting

To examine the spectral contents of the measured pulses, a window function (also known as the tapering function) is used to extract a particular pulse from the original one. The amplitude of the windowing function is zero everywhere except along a finite time interval with unitary amplitude, defined as the width of the window. The product of the windowing function and the original pulse results in the desired isolated

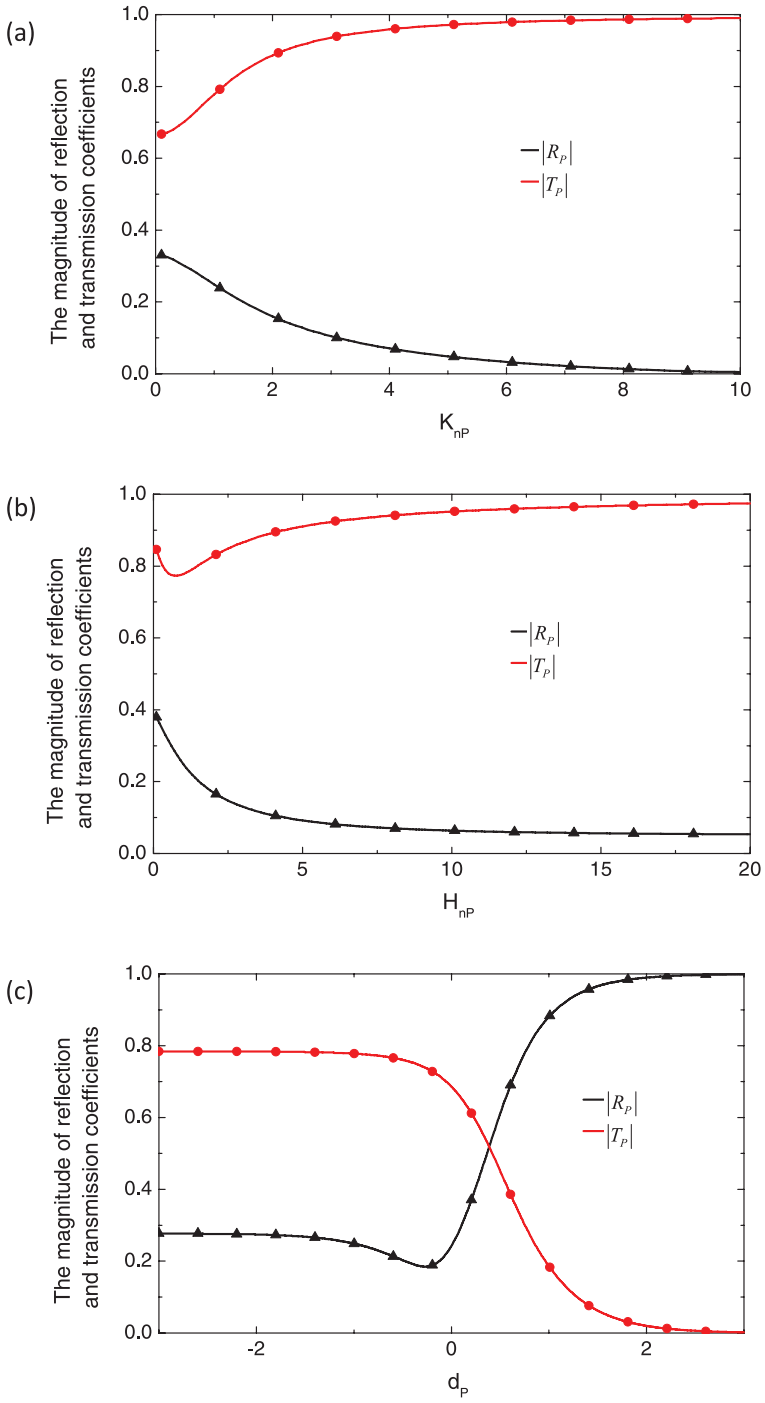

Figure 4. Reflection and transmission coefficients across a Kelvin joint versus (a) the non-dimensional joint stiffness, where $H_n = 1$ and $d = 0.1$; (b) the non-dimensional joint viscosity, where $K_n = 1$ and $d = 0.1$; (c) the impedance ratio of the filled joint, where $K_n = 1$ and $H_n = 1$, for normal P-wave incidence.

pulse. It should be noted that the same windowing function is used for the measured incident and transmitted waves to ensure that the results of the spectral contents are comparable with each other. In this study, Hann window, whose function is $0.5 \times \{1 - \cos[2\pi n/(N-1)]\}$, where n varies from 0 to $N - 1$, is used as the window function (Harris 1978). The amplitude spectra are then calculated by performing a fast Fourier transform (FFT) on the tapered waveforms, as shown in Fig. 10.

To achieve the best fit between the measured transmitted wave and the predicted transmitted wave derived from the analytical solutions, an algorithm that minimizes the least-squares differences between the two series of values is used. With iterative computations, the best fit mechanical parameters of the joint are determined as follows: $k_n = 33.748$ GPa m^{-1}, $\eta_n = 1.2919$ MPa s m^{-1} for the Kelvin model (Fig. 10a); $k_n = 31.566$ GPa m^{-1}, $\eta_n = 150$ MPa s m^{-1} for the Maxwell model (Fig. 10b).

It can be seen from Fig. 10 that the analytical solutions from both the Kelvin and the Maxwell models agree well with the experimental results. Therefore, the Kelvin and the Maxwell models can both be used to describe the seismic response of joints filled with sand for

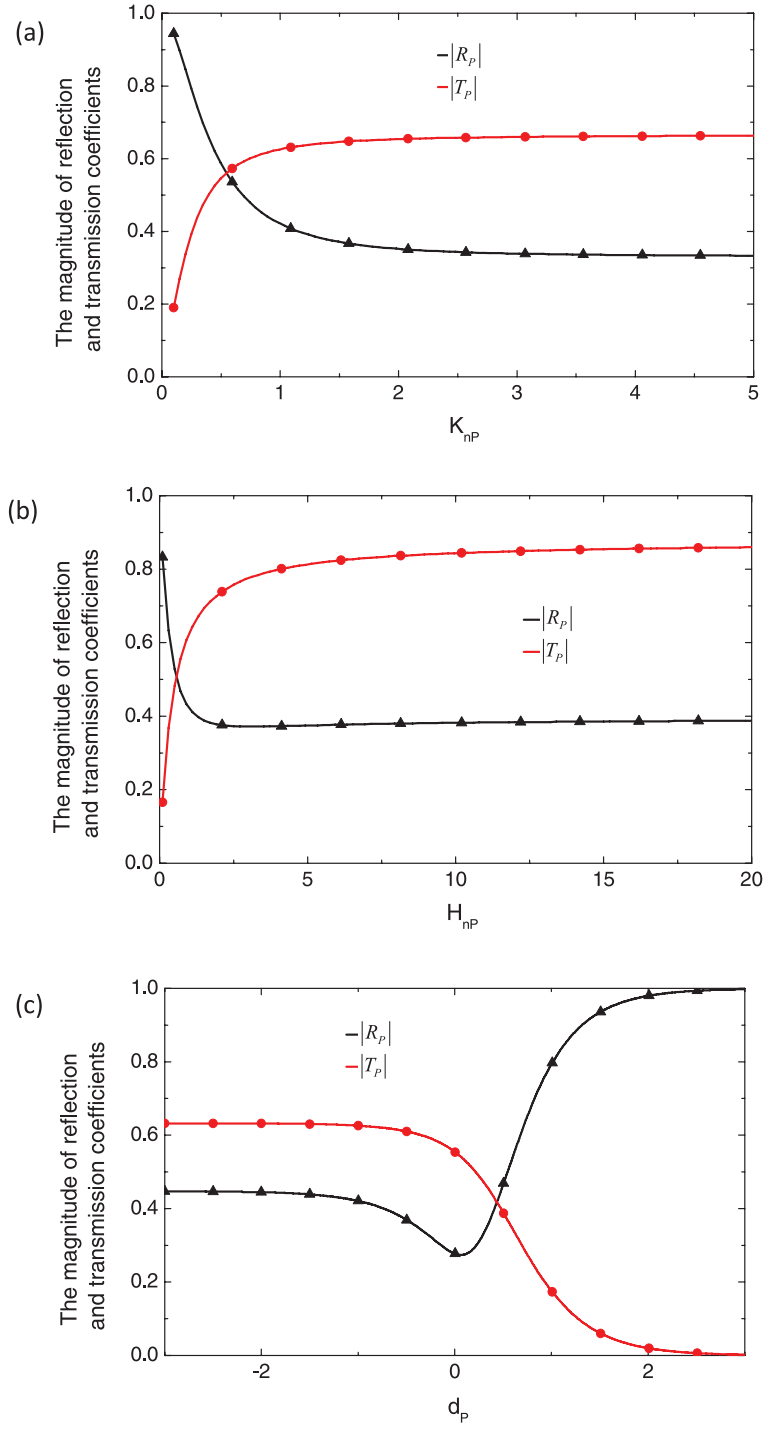

Figure 5. Reflection and transmission coefficients across a Maxwell joint versus (a) the non-dimensional joint stiffness, where $H_n = 1$ and $d = 0.1$; (b) the non-dimensional joint viscosity, where $K_n = 1$ and $d = 0.1$; (c) the impedance ratio of the filled joint, where $K_n = 1$ and $H_n = 1$, for normal *P*-wave incidence.

P-wave incidence. In addition, like the displacement discontinuity model, the filled joint model presented in this study also functions as a high-frequency filter. The high-frequency components across the joint attenuate much more than the low-frequency components.

4 WAVE PROPAGATION ACROSS A FILLED JOINT SET

Wave propagation across a joint set is more complicated due to the multiple wave reflections among joints. With the same joint mechanical parameters as mentioned earlier, normally incident *P*-wave propagation across a filled Kelvin joint set and a filled Maxwell joint set is studied in the following. For *S*-wave incidence, the changing trend is the same as that for *P*-wave incidence. The virtual wave source method (VWSM)

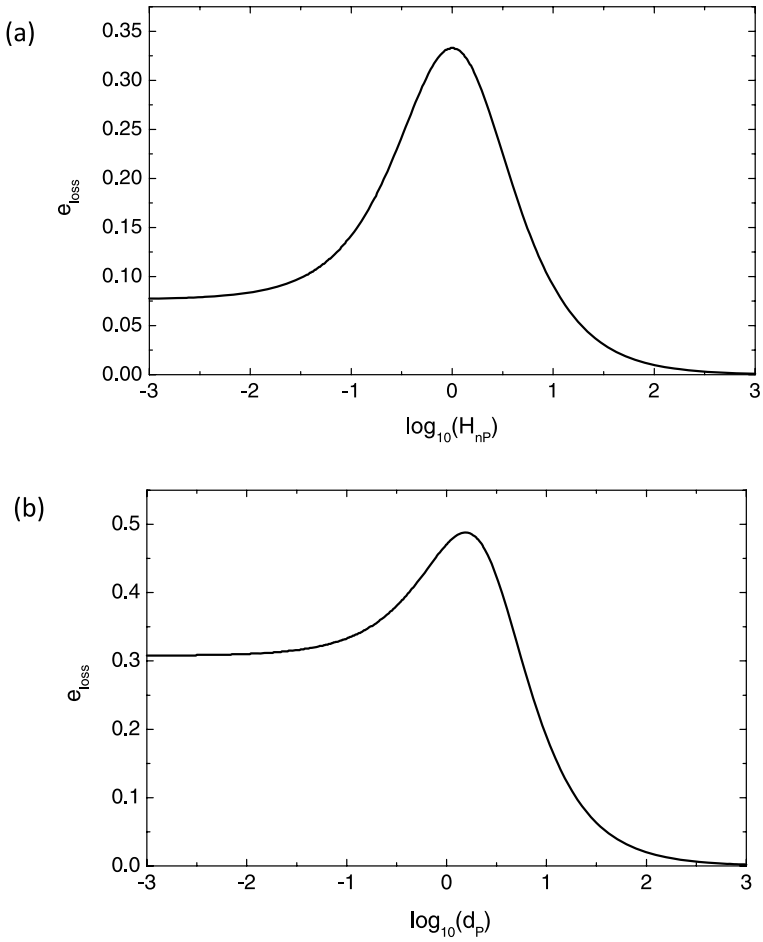

Figure 6. The energy loss ratio across a Kelvin joint versus (a) the non-dimensional joint viscosity, where $K_n = 1$ and $d = 0.1$; (b) the impedance ratio of the filled joint, where $K_n = 1$ and $H_n = 1$, for normal *P*-wave incidence.

and the scattering matrix method (SMM) are used to obtain the transmitted wave across a filled joint set, where multiple wave reflections are taken into account. The results obtained are compared and validated.

4.1 The VWSM

Combined with the equivalent medium model, Li *et al.* (2010) introduced a concept of virtual wave source (VWS) to obtain the equivalent viscoelastic moduli of the jointed rock mass.

Zhu *et al.* (2011) extended VWSM to study joint described by the displacement discontinuity model. Combined with the discontinuous model, VWS exists at the joint position and represents the mechanical properties of the joint. Each time when an incident wave propagates across the joint (VWS), VWS produces one or two reflected waves and one or two transmitted waves depending on the incident wave directions and types, which can be directly derived by using the reflection and transmission coefficients obtained earlier. The transmitted wave across a joint set is the result of wave superposition of different transmitted waves created by VWSs. To obtain the transmitted wave of the incident transient wave, FFT and inverse FFT are used to transform between frequency domain and time domain. Detailed description of VWSM can be found in the reference of Zhu *et al.* (2011).

4.2 The SMM

The scattering phenomenon that takes place when an elastic wave impinges on a discontinuity can also be analysed by the SMM (Aki & Richards 2002; Perino *et al.* 2010), which is borrowed from the study of electromagnetic wave propagation and the theory of transmission lines such as coaxial cables, optical fibres and strip-lines (Collin 1992).

In the case of a joint, incident, reflected and transmitted plane waves have the same transverse wave vector and the respective amplitudes are related by a 2×2 block matrix as follows:

$$\begin{pmatrix} \mathbf{c}_1^- \\ \mathbf{c}_2^+ \end{pmatrix} = \begin{pmatrix} \mathbf{S}_{11} & \mathbf{S}_{12} \\ \mathbf{S}_{21} & \mathbf{S}_{22} \end{pmatrix} \begin{pmatrix} \mathbf{c}_1^+ \\ \mathbf{c}_2^- \end{pmatrix}, \tag{35}$$

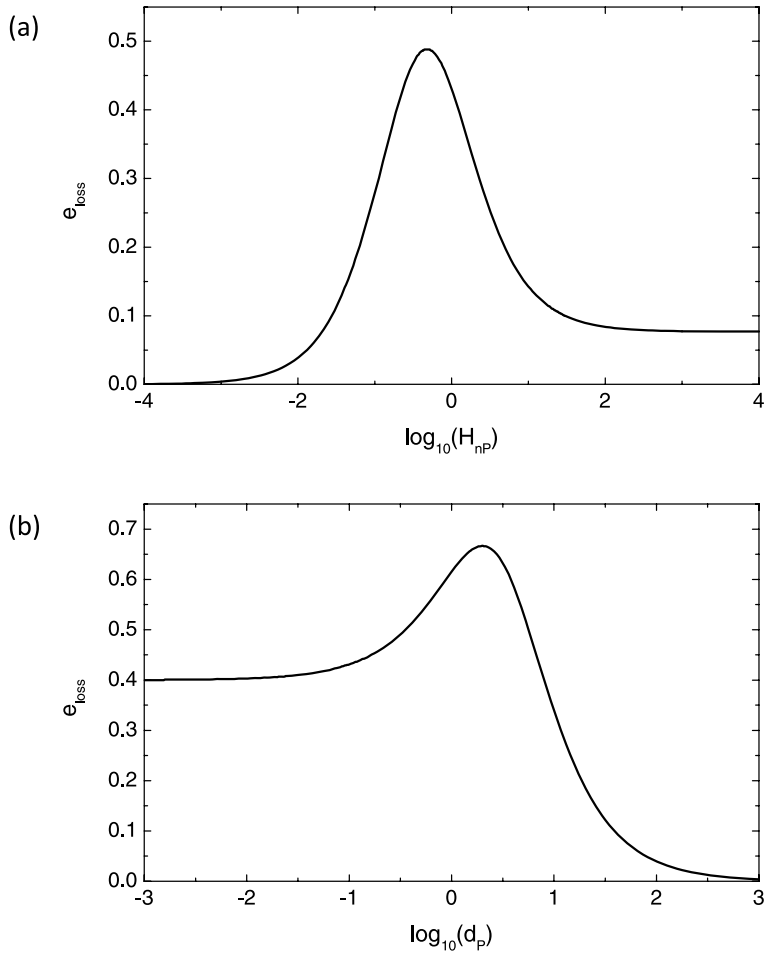

Figure 7. The energy loss ratio across a Maxwell joint versus (a) the non-dimensional joint viscosity, where $K_n = 1$ and $d = 0.1$; (b) the impedance ratio of the filled joint, where $K_n = 1$ and $H_n = 1$, for normal *P*-wave incidence.

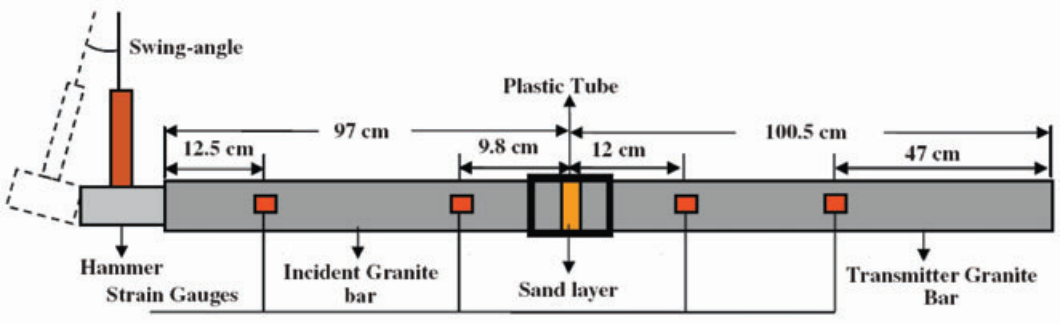

Figure 8. The configuration of the modified split Hopkinson pressure bar (SHPB) test.

where c_1^+ and $\mathbf{c}_2^-$ are the amplitudes of the waves incident on the joint, whereas $\mathbf{c}_1^-$ and $\mathbf{c}_2^+$ are the amplitudes of the scattered waves (reflected and transmitted), $\mathbf{S}_{ii}$ have the meaning of reflection coefficients at the two sides of the joint, and $\mathbf{S}_{ij}$ have the meaning of transmission coefficients. Since elastic waves have three possible polarization states (*P*, *SV*, *SH*), the submatrices have a size of 3×3. The values of $\mathbf{S}_{ii}$ and $\mathbf{S}_{ij}$ can be derived with the analitical solutions obtained in Section 2.

To extend the SMM to the case of *N* parallel joints, one may compute the scattering matrix for each of them. Then, by using a 'chain rule' procedure, the global scattering matrix is defined. This is a combination of the components of the scattering matrix for each joint and represents the effect on elastic wave propagation due to the *N* discontinuities. The global scattering matrix contains the global reflection and transmission coefficients of a joint set, where multiple wave reflections among the joints are taken into account.

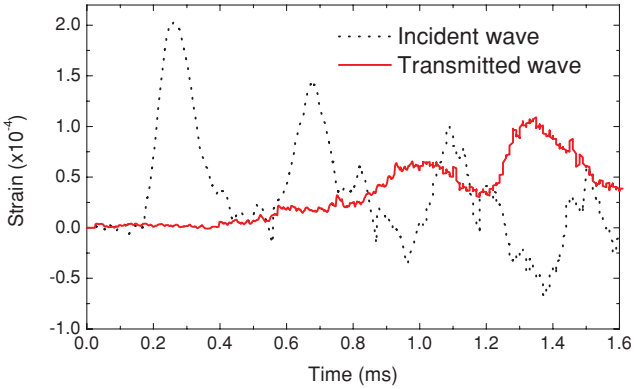

Figure 9. The measured incident and transmitted wave signals of the modified SHPB test.

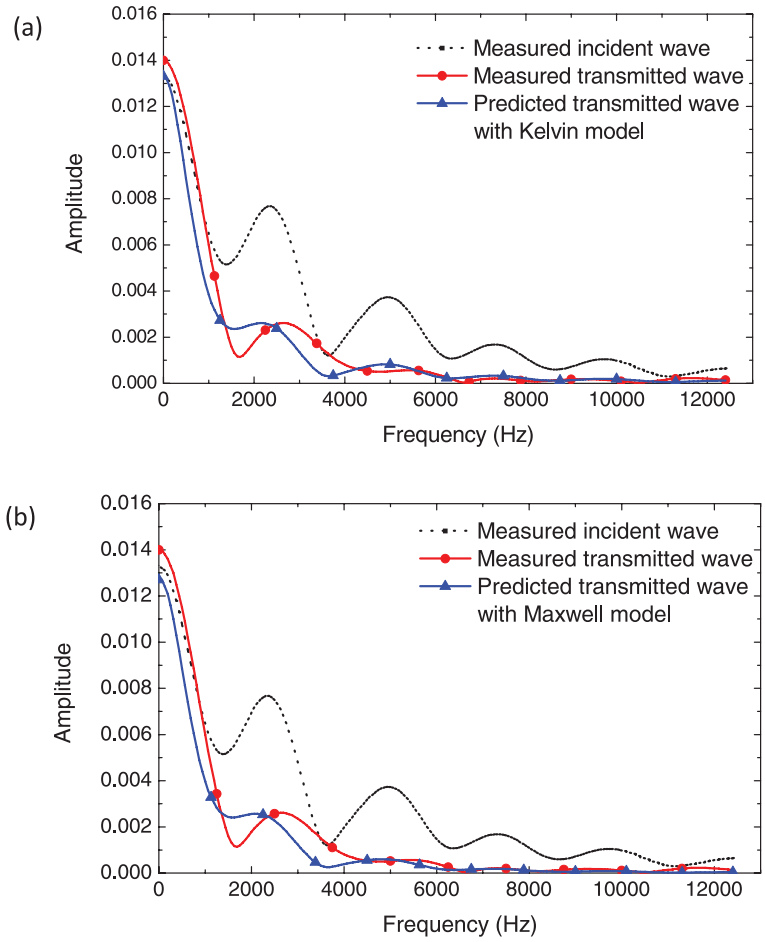

Figure 10. Spectra of the measured incident wave, measured transmitted wave and transmitted wave predicted with (a) the Kelvin model; (b) the Maxwell model.

4.3 Parametric studies

Without losing generality, a normally incident half-cycle sinusoidal *P* wave is assumed to be applied at the boundary of a filled joint set with viscoelestic behaviour, that is,

$$v_I(t,0) = \begin{cases} I\sin(\omega_0 t) \\ 0 \end{cases}, \quad \text{when} \quad \begin{matrix} 0 \le t \le \pi/\omega_0 \\ \text{others} \end{matrix}, \tag{36}$$

where I is the amplitude of the incident wave which is assumed to be one, ω_0 is the angular frequency of the incident wave which is taken as 2π KHz. The properties of the rock and of the filled material are the same as those of the experiment described in the previous section. The specific joint stiffness and viscosity of the Kelvin and Maxwell joints are those determined through the best fit of the experimental data described in the same section.

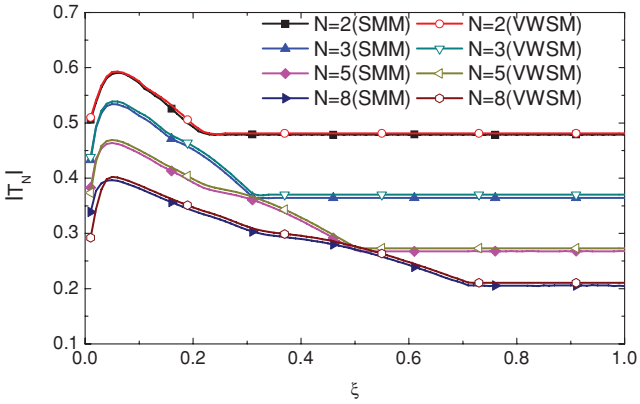

Figure 11. Transmission coefficients across N ($N = 2, 3, 5, 8$) Kelvin joints versus non-dimensional joint spacing (ξ) with VWSM and SMM.

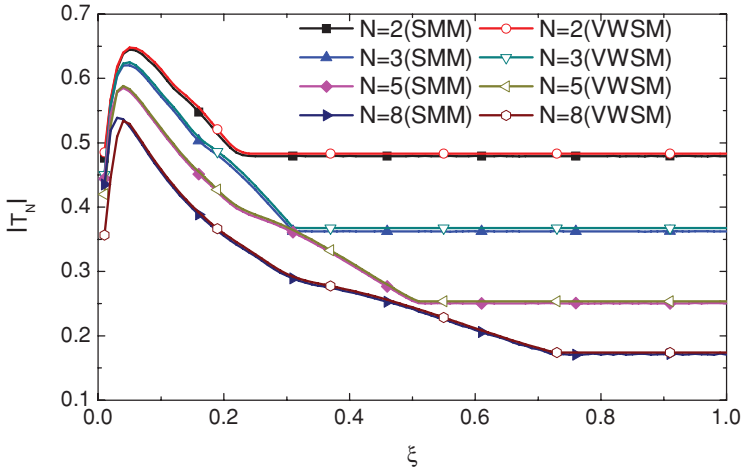

Figure 12. Transmission coefficients across N ($N = 2, 3, 5, 8$) Maxwell joints as a function non-dimensional joint spacing (ξ) with VWSM and SMM.

Figs 11 and 12 show the magnitude of transmission coefficients across N ($N = 2, 3, 5, 8$) Kelvin joints and N Maxwell joints ($|T_N|$), respectively, versus the non-dimensional joint spacing (ξ) based on VWSM and SMM. The non-dimensional joint spacing is defined as the ratio of the joint spacing to the incident wavelength, which is equal to $2\pi C_P/\omega_0$.

It is found that the results obtained by VWSM and SMM agree well with each other. Therefore, the capability of these two methods to study wave propagation across multiple viscoelastic joints is verified.

It is also found that although the general changing trend of $|T_N|$ versus ξ is the same for the Kelvin and Maxwell joints, the amplitudes are somewhat different. It indicates that even though both the Kelvin and the Maxwell models can be used to study *P*-wave propagation across a single viscoelastic joint filled with sand, the seismic response of multiple parallel Kelvin and Maxwell joints is somewhat different. Further experiments on wave propagation across multiple parallel joints filled with saturated sand are needed to determine which model is to be preferred.

It is noted that for both the Kelvin and Maxwell joints, $|T_N|$ first increases to the maximum value, with increasing ξ, before it decreases to a constant. It is also shown that when ξ is sufficiently large, it has no effect on $|T_N|$, which indicates that the multiple wave reflections among joints have no effect on $|T_N|$. This is because the arriving time difference between the first transmitted wave and later transmitted waves from multiple wave reflections is large enough to eliminate the influence of later arriving transmitted waves on $|T_N|$. While ξ is small, the multiple wave reflections among joints have great effects, and $|T_N|$ is dependent on ξ. It is also noted that $|T_N|$ decreases with the number of joints increasing.

5 DISCUSSION

Compared with other models, for example, the displacement discontinuity model, the displacement and stress discontinuity model is more suitable to study wave propagation across filled joints. The displacement and stress discontinuity model for the viscoelstic filled joint used in this study are approximated from the layered medium model (Brekhovskikh 1980), where the filled joint is a viscoelastic layer sandwiched between two elastic semispaces, and both displacements and stresses across the two interfaces of the filled joint are continuous. The initial masses of the filled joint are reflected by the non-dimensional parameter d in the process to obtain the reflection and transmission coefficients in eqs (24), (27) and (29)–(34). d can be regarded as the ratio of effective impedance of the filled viscoelastic medium to the acoustic

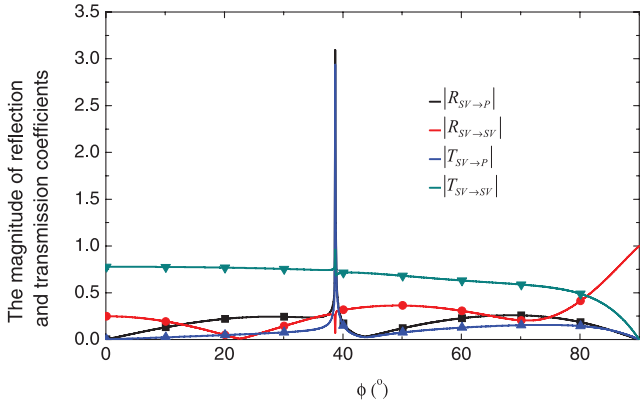

Figure 13. Reflection and transmission coefficients across a single Kelvin joint versus a full range of incident angles (from 0° to 90°) for *SV*-wave incidence.

impedance of the background rock. Also, according to the layered medium model, the wave reflection and transmission across each of the two interfaces of the filled joint are determined by the ratio of the impedance of the sandwiched layer to that of the semispace. Therefore, d is a key parameter to relate the boundary conditions used in this study, that is, the displacement and stress discontinuity model, to the layered medium model.

Instead of the specific joint viscosity η, which can be η_n or η_t, non-dimensional parameter H, which can be H_n or H_t, is adopted in this paper to simplify the mathematical expressions. It should be noted that different from K and d, H is frequency independent. This characteristic of η is significant when studying the reflected and transmitted waves and determining the joint properties in geophysics exploration and non-destructive evaluation studies.

Also of interest is to the physical meaning of η. The usually used viscosity is a property of the material and related to its particle velocity gradient. The specific viscosity used in this study depends on the particle velocity change between opposite sides of the joint. And therefore, this specific viscosity is a property of the joint.

In addition, η can result in wave energy dissipation. As shown in Figs 6 and 7, the energy loss caused by η is very small or zero when η is very small or very large; while η is close to 10, the wave dissipation is the largest. This characteristic of the specific joint viscosity is significant and can be applied to protective design of rock structures.

As proved in the paper, both of the Kelvin and the Maxwell models can be used to describe the viscoelastic behaviour of the filled joint. As well known, the Kelvin model is composed of a spring (reflected by K in the equations) and a dashpot (reflected by H in the equations) in parallel, while the Maxwell model is composed of a spring and a dashpot in series. Different configurations of the Kelvin and the Maxwell model result in different seismic responses. When either H or K approaches infinity, the Kelvin joint functions as a perfectly bonded interface, and no wave energy is reflected. However, only when both H and K approach infinity, the Maxwell joint can function as a perfectly bonded interface. When either H or K approaches zero, the Maxwell joint acts as a free surface, and no wave energy is transmitted. However, only when both H and K approach zero, the Kelvin joint is equivalent to a free surface.

Although interface waves are to be discussed in the future, some comments can also be made here. Based on eqs (22), (24) and (26), Fig. 13 shows the magnitude of reflection and transmission coefficients versus the incident angle, which varies from 0° to 90°, for an *SV*-wave incident upon a Kelvin joint. The other parameters adopted are the same as those in Fig. 2(b). It can be observed that $|R_{SV\to P}|$ and $|T_{SV\to P}|$ can be larger than 1.

6 CONCLUSIONS

The effects of filled joints of viscoelastic behaviour on wave propagation are of considerable fundamental significance and engineering interest. As the density of the filled medium, which is usually saturated clay or sand, is not negligible compared with the rock density, the displacement and stress discontinuity model is found to be suitable to reflect the seismic response of the filled joint.

The stress discontinuity across the filled joint is caused by the normal and tangential masses, which determine their acoustic impedance ratio. The displacement discontinuity across the filled joint results from the specific joint stiffness and viscosity, which further determine the non-dimensional joint stiffness and viscosity. It should be noted that the physical implication and unit of the specific joint stiffness and specific joint viscosity are different from those normally used.

The reflection and transmission coefficients across a single filled joint with viscoelatic behaviour are determined by parameters which include the incident angle, the non-dimensional joint stiffness, the non-dimensional joint viscosity and the impedance ratio of the filled joint. The impedance ratio of the filled joint and the non-dimensional joint stiffness are frequency dependent, while the non-dimensional joint viscosity is not. In addition, the wave energy is dissipated due to the viscosity and the initial mass of the filled joint.

The Kelvin and the Maxwell models, based on modified SHPB tests and curve fitting, are found to describe well the seismic response of viscoelastic joints filled with sand for *P*-wave incidence. The most relevant difference between the seismic responses of the Kelvin and the Maxwell joint depends on the different role the non-dimensional joint stiffness and the non-dimensional joint viscosity play in wave reflection

and transmission. When a wave propagates across a filled joint set, due to the presence of multiple wave reflections, the non-dimensional joint spacing is the dominating parameter.

ACKNOWLEDGMENTS

This research is financially supported by the Swiss National Science Foundation (SNSF) and the China Scholarship Council (CSC). Also to be acknowledged is the support of the Italian Ministry of Education, University and Research (MIUR).

REFERENCES

Aki, K. & Richards, P.G., 2002. *Quantitative Seismology,* University Science Books, Mill Valley, CA.

Brekhovskikh, L.M., 1980. *Waves in Layered Media,* Academic Press, New York, NY.

Cai, J.G. & Zhao, J., 2000. Effects of multiple parallel fractures on apparent attenuation of stress waves in rock masses, *Int. J. Rock Mech. Min. Sci.,* **37,** 661–682.

Collin, R., 1992. *Foundations for Microwave Engineering,* McGraw-Hill, New York.

Das, B.M. & Ramana, C.V., 2011. *Principles of Soil Dynamics,* Cengage Learning, Stamford, CT.

Fehler, M., 1982. Interaction of seismic-waves with a viscous-liquid layer, *Bull. seism. Soc. Am.,* **72,** 55–72.

Gu, B.L., Suárez-Rivera, R., Nihei, K.T. & Myer, L.R., 1996a. Incidence of plane waves upon a fracture, *J. geophys. Res.,* **101,** 25 337–25 346.

Gu, B.L., Nihei, K.T., Myer, L.R. & Pyrak-Nolte, L.J., 1996b. Fracture interface waves, *J. geophys. Res.,* **101,** 1107–1110.

Harris, F.J., 1978. Use of windows for harmonic-analysis with discrete Fourier-transform, *Proc. IEEE,* **66,** 51–83.

Hudson, J.A., Liu, E.R. & Crampin, S., 1996. Transmission properties of a plane fault, *Geophys. J. Int.,* **125,** 559–566.

King, M.S., Myer, L.R. & Rezowalli, J.J., 1986. Experimental studies of elastic-wave propagation in a columnar-jointed rock mass, *Geophys. Prospect.,* **34,** 1185–1199.

Li, J.C. & Ma G.W., 2009. Experimental study of stress wave propagation across a filled rock joint, *Int. J. Rock Mech. Min. Sci.,* **46,** 471–478.

Li, J.C., Ma, G.W. & Zhao, J., 2010. An equivalent viscoelastic model for rock mass with parallel joints, *J. geophys. Res.,* **115,** B03305, doi:10.1029/2008JB006241.

Perino, A., Barla, G. & Orta, R., 2010. Wave propagation in discontinuous media, in *Rock Mechanics in Civil and Environmental Engineering,* Proceedings of European Rock Mechanics Symposium (EUROCK) 2010, ed. Zhao, J., Labiouse, V., Dudt, J.-P. & Mathier, J.-F., CPC Press, Boca Raton, FL.

Pyrak-Nolte, L.J., Myer, L.R. & Cook, N.G.W., 1990. Transmission of seismic-waves across single natural fractures, *J. geophys. Res.,* **95,** 8617–8638.

Rokhlin, S.I. & Wang, Y.G., 1991. Analysis of boundary conditions for elastic wave interaction with an interface between two solids, *J. acoust. Soc. Am.,* **89,** 503–515.

Schoenberg, M., 1980. Elastic wave behavior across linear slip interfaces, *J. acoust. Soc. Am.,* **68,** 1516–1521.

Schoenberger, M. & Levin, F.K., 1974. Apparent attenuation due to interbed multiples, *Geophysics,* **39,** 278–291.

Suárez-Rivera, R., 1992. The influence of thin clay layers containing liquids on the propagation of shear waves, *PhD thesis,* University of California, Berkeley.

Verruijt, A., 2010. *An Introduction to Soil Dynamics,* Springer, Dordrecht.

Zhao, J., 1996. Construction and utilization of rock caverns in Singapore, part A: bedrock resource of the Bukit Timah granite, *Tunn. Undergr. Sp. Tech.,* **11,** 65–72.

Zhao, J., Cai, J.G., Zhao, X.B. & Li, H.B., 2006a. Experimental study of ultrasonic wave attenuation across parallel fractures, *Geomech. Geoeng.,* **1,** 87–103.

Zhao, X.B., Zhao, J. & Cai, J.G., 2006b. P-wave transmission across fractures with nonlinear deformational behaviour, *Int. J. Numer. Anal. Methods Geomech.,* **30,** 1097–1112.

Zhao, X.B., Zhao, J., Hefny, A.M. & Cai, J.G., 2006c. Normal transmission of S-wave across parallel fractures with Coulomb slip behavior, *J. Eng. Mech.-ASCE,* **132,** 641–650.

Zhu, J.B., Zhao, X.B., Zhao, G.F., Li, J.C. & Zhao, J., 2011. Normally incident wave propagation across a joint set with virtual wave source method. *J. appl. Geophys.,* **73,** 283–288.